10.1109/ULTSYM.2009.0198

Unraveling Interfacial Jetting Phenomena Induced by Focused Surface Acoustic Waves

James Friend, Ming Tan and Leslie Yeo
MicroNanophysics Research Laboratory
Department of Mechanical and Aerospace Engineering
Monash University
Melbourne Australia 3800
Email: james.friend@eng.monash.edu.au

***Abstract*—Surface acoustic waves have been known to be able to drive fluid jetting phenomena, though the underlying physical mechanism has remained unclear. In a setup designed to reliably jet small fluid droplets, a pair of focused single-phase unidirectional transducers were placed facing each other along the x-axis of a 128° Y–X lithium niobate substrate. Driving both transducers at the same time, the laterally focused acoustic energy appears beneath a drop placed on the surface, refracting into the drop and causing destabilization of the drop's free surface. Above a critical Weber number We, an elongated jet forms for drops with dimensions greater than the fluid sound wavelength. Further increases in We leads to single droplet pinch-off and subsequent axisymmetric break-up to form multiple droplets. Derivation of a simple relationship based on the acoustics and fluid physics predicts the jetting behavior across a wide range of Newtonian fluids, droplet sizes, and input powers.**

Beyond a critical Weber number, a liquid drop can form into a *jet* when sufficient fluid inertia exists to overcome the restoring capillary stresses acting on its free fluid surface [1]. Presuming the Weber number criterion is met, delivering sufficient inertia to form such a jet often requires a mechanism to confine the fluid such as a nozzle or orifice. In surface acoustic wave (SAW) jetting, no such confinement is needed; generation of a liquid jet ejecting up to 1–2 cm from the *free surface* of a sessile drop is possible. The key to the generation of such jetting phenomena is the concentration of mechanical energy into the drop made possible by surface acoustic waves.

We employ SAW Rayleigh waves; SAWs and their energy are essentially confined to a depth of 3–4 wavelengths into the substrate, and the energy associated with these waves may be further concentrated to a spot roughly equivalent to the wavelength of the radiation using focusing transducers [2]–[4]. In doing so, large surface accelerations are formed—beyond 10^7 m/s^2—serving to destabilize the air-fluid interface of a drop set atop this surface and hence produce a single elongated column of liquid. This is in distinct contrast to the behavior induced by long-wavelength, in-phase piston vibration of a drop which can only atomize the drop via the formation and bursting of large numbers of short liquid spikes on the drop's surface [5]. A similar focusing concept but significantly different mechanism using a relatively large spherically converging acoustic beam has been employed to eliminate the use of nozzles [6]; the short focal depths result in short (< 1 mm) jets which quickly pinch-off to form an ejected droplet. Here, however, the acoustic radiation travels over a longer length scale in the fluid due to the SAW. SAW-driven jets have appeared in the past [7], but little of the associated physics has been explored.

The SAW is generated by applying a sinusoidal electric voltage to a *focusing* electrode-width-controlled single-phase unidirectional interdigital transducer (EWC-SPUDT) [8] fabricated on a 0.5-mm thick 128° *y–x* lithium niobate (LN) single crystal piezoelectric substrate (Fig. 1(a)) using standard UV photolithography [4]. Any spurious waves generated by the system were absorbed by placement of polydimethylsiloxane (α-gel, GelTec Ltd., Japan) around the periphery of the device. Details on the fabrication of the IDT are documented elsewhere [2], [9]; the SAW wavelength was $\lambda_{\mathrm{SAW}} \approx 200$ μm with a fundamental resonance frequency $f \approx 20$ MHz. Since the sound velocity in water is far lower, $c_l \approx 1495$ m/s, about 33% of the SAW acoustic energy refracts into the liquid drop at the *Rayleigh angle* $\theta_{\mathrm{SAW}} = \sin^{-1} c_l/c_s \approx 23°$. At sufficient intensities, the so-called *leaky* SAW in the liquid, in turn, generates *acoustic streaming* and bulk flow within the drop [4], [10], [11], with the air-water interface representing a reflective boundary for the acoustic radiation due to the large acoustic impedance difference across it.

At relatively low applied powers and hence low surface acceleration $|\ddot{\xi}_{x_3}|$, where $\ddot{\xi}$ represents the second-order time derivative of the substrate's surface displacement ξ and x_3 the direction perpendicular to the substrate, weak acoustic streaming will occur in a drop of a size much greater than the acoustic wavelength in the fluid, i.e., $R_d \gg \lambda_f \sim 73$ μm for $f \approx 30$ MHz. However, as the drop sizes shrink, capillary stresses begin to dominate and capillary waves begin to appear on the drop interface. As the drop becomes progressively smaller, the intensity of these vibrations grows (provided $R_d \gg \lambda_c \sim 1$ μm, which is the capillary wavelength) while the streaming weakens as a result of the increasing surface-to-volume ratio as R_d decreases; the capillary waves depend upon the surface area while the acoustic streaming depends upon the volume. When $R_d \approx \lambda_f$, the streaming within the drop ceases.

With increasing power, the increasing surface acceleration magnitude on the substrate $|\ddot{\xi}_{x_3}|$ leads to stronger fluid streaming, as characterized by the streaming Reynolds number

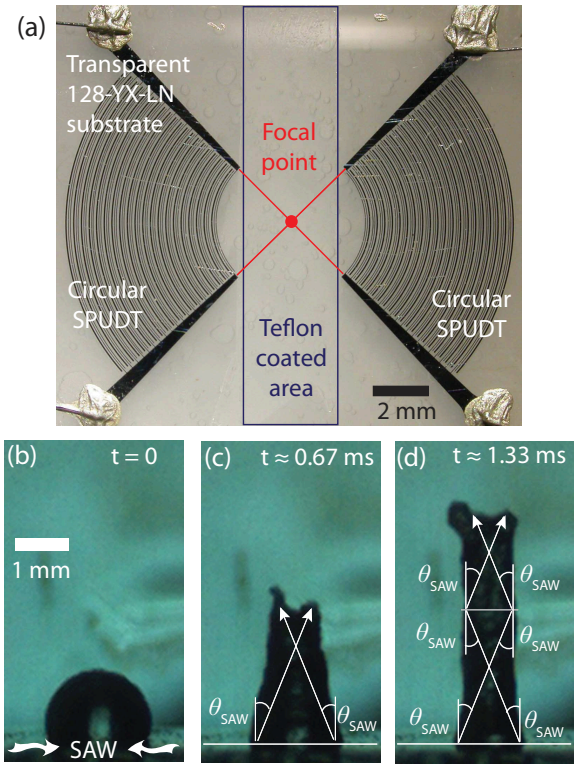

Fig. 1. Image (a) shows two circular focusing electrode-width-controlled SPUDTs fabricated at the ends of a LN substrate to provide the focused SAWs whose radiation into the drop placed on the substrate causes it to deform into a coherent elongated jet as shown in images (b)–(d). The water-air interface reflects the acoustic radiation up the fluid column as it extends, as depicted in image (d). The drop is placed at the focal point between the two EWC-SPUDTs within an area coated with a thin (< 1 μm) layer of Teflon to render the hydrophilic LN substrate hydrophobic.

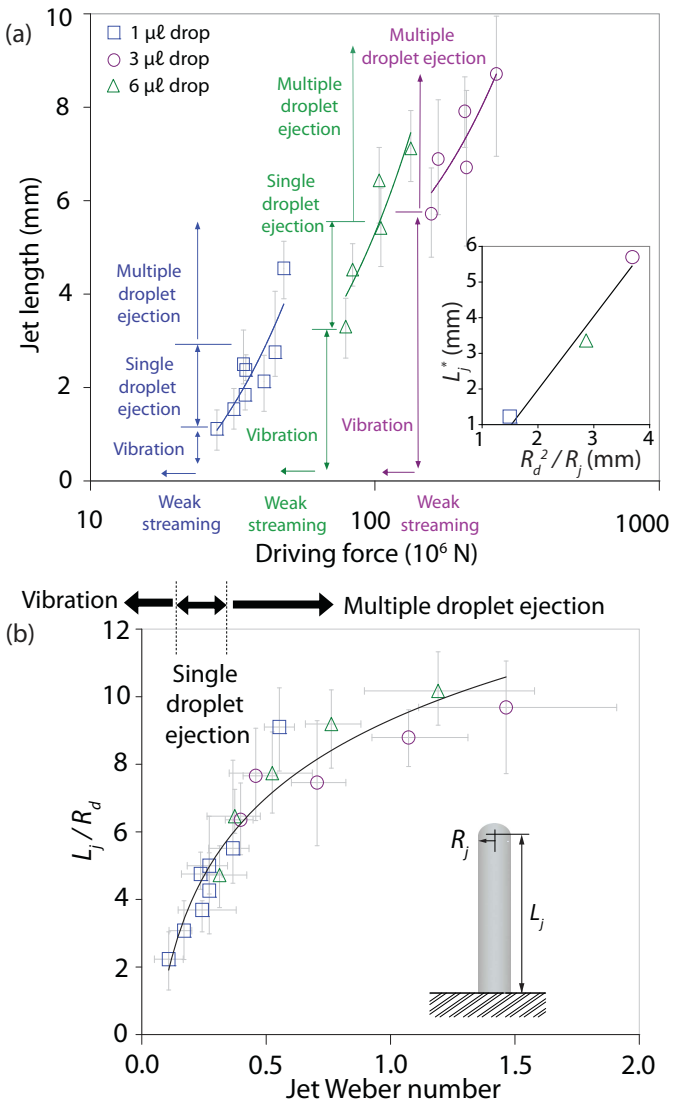

Fig. 2. (a) Jet length as a function of the applied driving force. The inset shows the jet length at the onset of the phenomena at the instant when the threshold force is exceeded L_j^* (the jet length at the smallest value of the driving force when jetting is first observed) and its relationship to the parent drop size. (b) Dimensionless jet length as a function of the jet Weber number. We note the transitions for both the onset of jetting from drop vibration and between single and multiple droplet ejections occur at Weber numbers of 0.1 and 0.4, respectively.

$\mathrm{Re_s} \equiv \rho U_s R_d/\mu$, where ρ and μ are the liquid density and viscosity, respectively, and U_s is the characteristic streaming velocity. For $\mathrm{Re_s} \sim 1$, $U_s \sim 10^{-3}$ m/s. Bulk vibration of the drop is also observed when a standing SAW is employed. At these powers, the acoustic streaming in the drop generates sufficient body force to overcome contact line pinning, and the drop begins to translate if the SAW is propagating [2]. With further increases in $|\ddot{\xi}_{x_3}|$, the inertial streaming ($\mathrm{Re_s} \sim 10^3$) can no longer be dissipated by viscous or capillary means, and the drop either deforms into an elongated liquid jet or atomizes [9]. At a given value of $|\ddot{\xi}_{x_3}|$, we observe jets to form in the inertia-dominant regime when $R_d \gg \lambda_f$ while atomization [12] is particularly prominent in the capillary force dominant regime when $R_d < \lambda_f$.

Restricting ourselves to the peculiar jetting phenomenon, we employ a pair of the EWC-SPUDTs (hereafter simply referred to as the "electrodes") as shown in Fig. 1(a) to generate a pair of Rayleigh surface acoustic waves converging to the focal point as indicated; the transducers are placed such that the x-axis of the 127.68° lithium niobate substrate is along the horizontal direction in the figure. To increase the static contact angle between the deionized water drop (here, 1, 3 and 5 μl drop volumes V_d are employed) and the substrate surface, we coat an area on the substrate in between the electrodes, as shown in Fig. 1(a), with a 100 nm thick layer of Teflon (Teflon AF, DuPont Corp., USA). The jetting dynamics were captured at 500 to 2000 fps using a high speed video camera (iSpeed, Olympus, Japan) mounted onto a long-distance microscope (K2, InfiniVar, USA). Measurements of the surface acceleration $\ddot{\xi}_{x_3}$ were obtained through scanning laser Doppler vibrometry (LDV) (MSA-400, Polytec PI, Germany) focused directly on the substrate. Figure 2(a) shows the jet length prior to its break up into droplets as a function of the driving force $F = \rho V_d \ddot{\xi}_{x_3}$; the large amplitude of the force is due to the high surface accelerations generated by the SAW. At

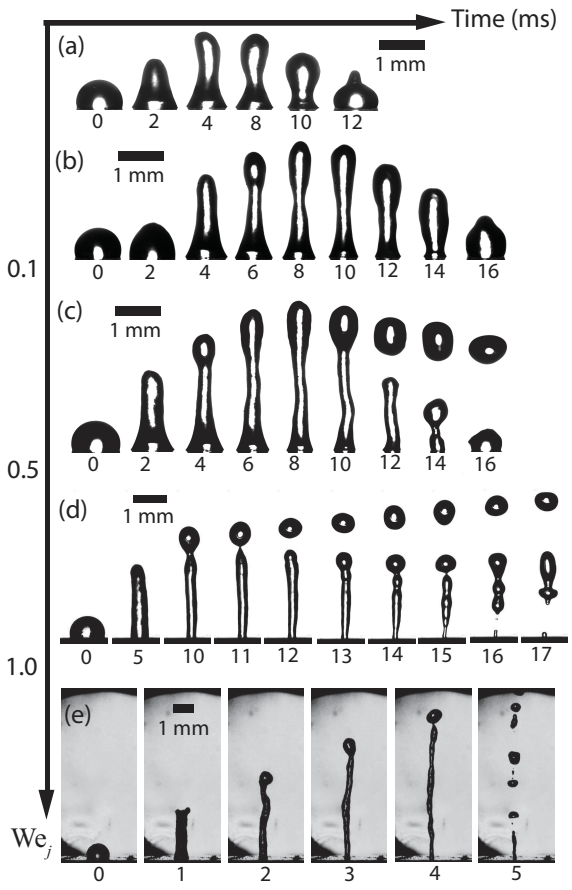

Fig. 3. Experimental images showing the transition from (a) drop vibration to (b) jetting, (c) pinch-off of a single droplet, and, (d,e) jet break-up to form multiple droplets by increasing the jet Weber number We_j.

the input power levels employed, the surface displacement velocity $\dot{\xi}_{x_3}$ is around 1 m/s irrespective of the SAW excitation frequency. So while the surface displacement ξ_{x_3} and hence the SAW amplitude is only around 10 nm at these 10 MHz order frequencies, the surface acceleration is on the order of 10^8 m^2/s [9]. It is these extremely large accelerations and hence forces which are transmitted into the drop through an area on the order of λ_{SAW} in size via radiation focusing that gives rise to the jetting phenomena. There exists a threshold value for the force that, once exceeded, causes jetting; the larger the parent drop, the larger the threshold value. Below the threshold, the drop merely vibrates with an amplitude proportional to the force, since there is insufficient inertial stress to overcome the surface tension of the drop. In fact, the threshold value for the force at the onset of jetting actually sets the jet length. At the onset of jetting, a balance between the surface energies of the parent drop, assumed hemispherical due to the hydrophobic substrate, and the jet, assumed to resemble a cylindrical column, then sets the length of the jet when it first appears from the conical apex of the vibrating drop after the threshold force is exceeded: $L_j^* \sim R_d^2/R_j$, in which R_j is the jet radius, consistent with that observed in the inset of Fig. 2(a).

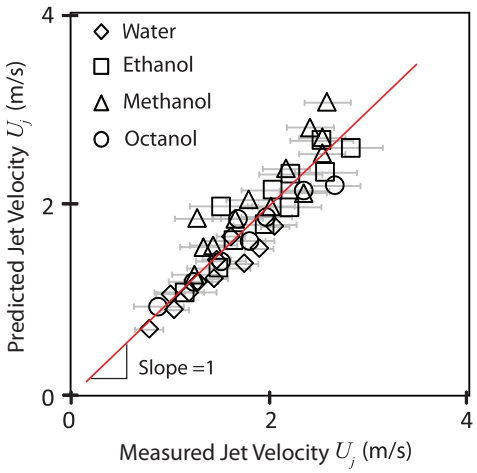

Fig. 4. Measured jet velocity versus predicted jet velocity based on Eq. (1) over a range of acoustic Reynolds numbers.

Figure 2(a) also documents evidence that at larger driving forces, the jet no longer pinches off at its leading edge to eject a single droplet. Instead, we see evidence of the classical Rayleigh-Plateau instability through which the cylindrical liquid column becomes unstable to axisymmetric perturbations with wavelengths several times larger than the R_j [13], [14], consequently breaking up to form multiple droplets. The transitions from the onset of jetting to the pinch-off of a single droplet and the break-up of the jet to form multiple droplets are more clearly observed by recasting the experimental data in terms of a jet Weber number $\mathrm{We}_j \equiv \rho U_j^2 R_j/\gamma$, where U_j is the velocity of the jet, as shown in Fig. 2(b). We observe the onset of jetting and the transition from single droplet pinch-off to multiple droplet formation as a consequence of the axisymmetric break-up of the jet to universally occur at Weber numbers of 0.1 and 0.4, respectively. Typical dynamics of the jet formation and the droplet ejection at different Weber numbers captured through high speed flow visualization are shown in Fig. 3.

By introducing an acoustic forcing term to the leading order axisymmetric jet momentum balance derived by Eggers [1], we arrive at the following relationship that permits the prediction of the axial jet velocity:

$$U_j \cong \sqrt{2L_j}\sqrt{F_{\mathrm{s}}^y - g}, \tag{1}$$

where $F_{\mathrm{s}}^y \approx \alpha_0 \beta \dot{\xi}_{x3}^2 \mathrm{Re}_{\mathrm{ac}}$ is the streaming force [15], g is the gravitational acceleration, $\alpha_0 = b\omega/(2\rho_f c_l^3)$ is the coefficient of acoustic attenuation, $\beta = 1 + B/2A$ is the coefficient of nonlinearity for the liquid [16] and the quantity B/A is proportional to the ratio of coefficients of the quadratic and linear terms in the Taylor series expansion of the equation of state [16], [17]. The quantity $\mathrm{Re}_{\mathrm{ac}} = \rho \dot{\xi}_{x3} \lambda_f/(2\pi b)$ is the acoustic Reynolds number [15], where $b = 4\mu/3 + \mu_{\mathrm{B}}$ and μ_{B} is the fluid bulk viscosity. Figure 4 shows the measured versus predicted jet velocity using Eq. (1) across different working fluids. We obtain good agreement throughout between the predicted and measured jet velocities.

I. Conclusions

Our study provides a complete physical basis for understanding the phenomena of SAW-driven jetting sufficient for using it in actual applications. Our device, employing a matched pair of EWC-SPUDTs, is an illustration of the potential use of the technology in microprinting not only inks but metals and other materials for rapid prototyping.

II. Acknowledgements

Support of this research by the Australian Research Council's Discovery Grant DP0773221 and Nanotechnology Victoria Grant BN–004 is gratefully acknowledged.

References

[1] J. Eggers, "Nonlinear dynamics and breakup of free-surface flows," *Reviews of Modern Physics*, vol. 69, no. 3, pp. 865–929, 1997.

[2] M. Tan, J. Friend, and L. Yeo, "Microparticle collection and concentration via a miniature surface acoustic wave deivce," *Lab on a Chip*, vol. 7, pp. 618–625, 2007.

[3] V. Laude, D. Gérard, N. Khelfaoui, C. Jerez-Hanckes, S. Benchabane, and A. Khelif, "Subwavelength focusing of surface acoustic waves generated by an annular interdigital transducer," *Applied Physics Letters*, vol. 92, p. 094104, 2008.

[4] R. Shilton, M. K. Tan, L. Y. Yeo, and J. R. Friend, "Particle concentration and mixing in microdrops driven by focused surface acoustic waves," *Journal of Applied Physics*, vol. 104, p. 014910, 2008.

[5] A. James, M. Smith, and A. Glezer, "Vibration-induced drop atomization and the numerical simulation of low-frequency single-droplet ejection," *Journal of Fluid Mechanics*, vol. 476, pp. 29–62, 2003.

[6] S. A. Elrod, B. Hadimioglu, B. T. Khuri-Yakub, E. G. Rawson, E. Richley, C. F. Quate, N. N. Mansour, and T. S. Lundgren, "Nozzleless droplet formation with focused acoustic beams," *Journal of Applied Physics*, vol. 65, no. 9, pp. 3441–3447, 1989. [Online]. Available: http://link.aip.org/link/?JAP/65/3441/1

[7] K. Chono, N. Shimizu, Y. Matsui, J. Kondoh, and S. Shiokawa, "Development of novel atomization system based on SAW streaming," *Journal of Applied Physics*, vol. 43, pp. 2987–2991, 2004.

[8] J. Hode, J. Desbois, P. Difilie, M. Solal, and P. Ventura, "SPUDT-based filters: design principles and optimization," in *Proceedings of the 1995 IEEE Ultrasonics Symposium*, vol. 1. Seattle, WA, USA: IEEE, 1995, pp. 39–50.

[9] A. Qi, L. Yeo, and J. Friend, "Interfacial destabilization and atomization driven by surface acoustic waves," *Physics of Fluids*, vol. 20, p. 074103, 2008.

[10] T. Frommelt, M. Kostur, M. Schäfer, P. Talkner, P. Hänggi, and A. Wixforth, "Microfluidic mixing via acoustically driven chaotic advection," *Physical Review Letters*, vol. 100, p. 034502, 2008.

[11] H. Li, J. Friend, and L. Yeo, "Colloidal island formation and erasure in a microfluidic system induced by surface acoustic wave radiation," *Physical Review Letters*, vol. 101, p. 084502, 2008.

[12] J. Friend, L. Yeo, D. Arifin, and A. Mechler, "Evaporative self-assembly assisted synthesis of polymeric nanoparticles by surface acoustic wave atomization," *Nanotechnology*, vol. 19, p. 145301, 2008.

[13] J. Plateau, "Statique expérimentale et théorique des liquides soumis aux seules forces moléculaires," *Acad. Sci. Bruxelles Mém.*, vol. 23, no. 5, 1849.

[14] L. Rayleigh, "On the capillary phenomena of jets," *Proceedings of the Royal Society of London*, pp. 71–97, 1879.

[15] L. D. Rozenberg, *High-Intensity Ultrasonic Fields*. Plenum Press., 1971.

[16] R. T. Beyer, *Nonlinear Acoustics*. Academic Press, 1998, ch. 2, pp. 25–40, eds.: Hamilton, M. F. and Blackstock, D. T.

[17] M. K. Tan, J. Friend, and L. Y. Yeo, "Interfacial jetting phenomena induced by focused surface vibrations," *Physical Review Letters*, vol. 103, no. 2, 2009.